

Growth model of a carbon based 3D structure (Aerographite) and electrical/mechanical properties of composites

J. Marx^{1*}, S. Garlof¹, J. Timmermann¹, D. Smazna², R. Adelung², K. Schulte^{1*}, B. Fiedler¹

¹*Institute of Polymer Composites, Hamburg University of Technology, Denickstr. 15, 21073 Hamburg*

²*Institute of Functional Nanomaterials, University of Kiel, Kaiserstr. 2, 24143 Kiel*

*janik.marx@tuhh.de, schulte@tuhh.de

Keywords: CFD simulation, CVD process, SEM, electrical properties, 3D reinforced composite

Abstract

Aerographite is a 3D interconnected carbon based tetrapod structure. The production of Aerographite can be divided in two steps. First, the production of zinc oxide (ZnO) templates in a flame transport synthesis followed by the replication into the carbon structure in a chemical vapor deposition process (rCVD). During the rCVD process carbon deposits on the surfaces of the zinc oxide template, with the simultaneous reduction of zinc oxide into gaseous zinc. This replication process starts from the tetrapod base and continues alongside the tetrapod arms towards its top. Based on interrupted synthesis processes investigated by intense scanning electron microscopy (SEM) we present a simple model of the growth mechanisms of Aerographite. In a CFD (Computational Fluid Dynamics) simulation we could demonstrate that the initial flow of the cold Ar and H₂ gas, when entering the reactor, sinks to the bottom, heats up to at the center of the reactor (where we have the maximum temperature) and advances to the top of the reactor. Vortexes are induced, leading to a partly backstream of the gas. The gas flow hits the samples from the back, so the conversion process of the zinc oxide templates starts from here towards the front of the samples. Furthermore, the electrical and mechanical properties of neat Aerographite and polymer composites will be shown.

1 Introduction

For the application of Aerographite it is essential to have a high quality and optimized structure with the requisite to understand in detail the underlying growth mechanisms. In course of the CVD process the conversion from ZnO to the 3D interconnected carbon structure occurs. The CVD process is one of the promising processes for the industrial production of Aerographite in which a carbon sources is injected into a streaming gas flow [3,4]. This perception can be achieved by a specific variation of the synthesis parameters, for example, the composition of the carbon source, its injection time and temperature, which all allow to adept the properties of these structures towards the required applications. In 1952, Radushkevich and Lukyanovich may have been the first to discover carbon nanotubes (CNTs) [5]. However, not until Iijima reported and described CNTs in 1991 [6], the science of CNTs boosted, leading to a worldwide hype, whereby the importance of clarifying the growth mechanism of such structures gained in importance. Iijima already published various models of the growth process of the CNT variants using ex-situ TEM observation [7,8]. Some groups also investigated the growth of graphene using ex-situ methods. In course of this, it was published that the growth of graphene is predominantly due to defects such as e.g. grain boundaries or corners [9,10]. New analysis methods, especially the environmental transmission electron microscopy (ETEM) now allow an in situ analysis of such growth

processes [11-13]. Although the ex-situ analyses is a powerful tool for the explanation of growth processes, the in situ analysis of such growth processes offers decisive advantages in the clarification of the influence of catalysts and the formation of defects [14-17]. As CNTs [3,4] also 3D crosslinked carbon structures can be produced via CVD processes [2,18]. The production of 3D carbon structures can be distinguished in template-based [2,18,19] and template-free [20] methods. The synthesis of Aerographite is a template-based method with tetrapodic zinc oxide (ZnO) as template. During the synthesis, the morphology of the tetrapodic template remains intact. For silicon layers, which are as well produced in the CVD process, it is well known that the growth starts at energetically favorable points [21]. The properties of Aerographite can be varied by different CVD parameters - for example the carbon injection rate - as the density, the morphology or the mechanical properties. Its structure can be distinguished between an open hollow, a closed-shell and a closed-shell and filled variant [2]. It is important to understand the growth mechanisms of Aerographite to design and tailor the properties of this structure towards specific applications. Up to now the predominant Aerographite variant "closed shell" has been of interest for a variety of applications, such as the growth of nerve cells [22], polymer composites [23,24] or sensors [25].

Further, 3D nanocarbon materials exhibit a high potential for improved electrical conductivity and mechanical reinforcement of polymer nanocomposites. The incorporation of 3D nanocarbons in a polymer matrix can circumvent several drawbacks in contrast to dispersed carbon nanoparticles [26-30], like agglomeration and lack of a controlled network topology, hence "ideal" composites can be created. Due to the presence of covalent interconnections (CVD grown 3D nanocarbons) or low tunneling distances (3D nanocarbon assemblies) direct pathways for electrical and thermal conduction are easily available [31-36].

In the present work, we show the fundamentals of the growth mechanism of Aerographite in consideration of a CFD simulation of the CVD process and their influence on the synthesis, based on interrupted synthesis processes followed by intense SEM observations. For the analysis of the flow conditions in a closed system, such as a CVD reactor, the CFD simulation is an appropriate method to understand the physical conditions in a CVD reactor. Furthermore, we present the electrical and mechanical properties of Aerographite/epoxy composites.

2 Materials and methods

2.1 Synthesis of Aerographite networks

The manufacturing of Aerographite is based on a two-step process. First the production of the zinc oxide template [1], followed by the second step in which the template is converted in a CVD process to the final 3D interconnected carbon structures [2].

The templates with a tetrapod structure are produced in a simple Flame Transport Synthesis. Metal micro-powders (Zn), with a particle size between 3 and 10 μm , are mixed with a polymer (Polyvinyl Butyral (-PVB)) in a ratio of 1:2 and heated up to 900 $^{\circ}\text{C}$ in a muffle oven. For the variation of the structure a mixture of the template powder, ethanol and PVB is also in the oven. Then the mixture is heated up above the autoignition temperature. The result of the production is a three dimensional interconnected tetrapodic zinc oxide network [1]. To achieve the final 3d graphitic structure (Aerographite) - second step - the templates are placed

in a CVD reactor. The reactor (Nabertherm, RS80/750/11) has a diameter of 80 mm and a length of 1300 mm, with an effective heatable zone of 750 mm. Samples with a volume of 1 cm³ are placed in the main zone (2) of the reactor in a well-defined position (3). Before the synthesis starts the reactor is heated up to 760 °C for 30 minutes with a continuous argon flow of 0.2 l/min. This is followed by the supply of hydrogen with a flow of 60 ml/min and the start of the synthesis with injecting toluene (C₇H₈, 99.5% Alfa Aesar) as carbon source into the 200 °C preheated injection zone (1) at an injection rate of 7.5 ml/h (1st phase). Usually, toluene is injected for 60 minutes. After the 760 °C phase follows a 900 °C phase for 1h (2nd phase), without the injection of the carbon source. The synthesis is stopped during the cooling down phase, without hydrogen but now at an argon gas flow of 0.4 l/min [2]. In order to better understand the mechanisms and processes occurring, the syntheses were regularly aborted several times during the 1st phase. An interrupted synthesis was not continued, but analyzed to investigate the changes of the structure.

2.2 Structure and morphology of Aerographite networks

The morphology and the growth of the carbon structure was characterized using a SEM (Zeiss Supra VP 55, acceleration voltage 5 kV) and the wall thickness was analyzed by using a TEM (FEI Talos F200X, acceleration voltage 200 kV). The TEM samples were prepared by dispersing the Aerographite in methanol (LC-MS >99.9%, Sigma Aldrich) via the ultrasonic sonotrode (Bandelin Sonoplus). The solution was treated for 10 seconds at 10% of the power. Aerographite was destroyed into small pieces remaining in the solution from which a droplet was positioned on the TEM sample holder using a syringe and then dried for 45 minutes at 80 °C on a heating plate.

2.3 CFD Simulation

The flow simulation was performed with ANSYS Fluent 17.0. A model of the inner wall of the reactor was first created in Autodesk Inventor 2017. All important parameters such as Reynolds, Prandtl, Mach, Grashof, Nußelt and Rayleigh number were calculated analytically. A mesh of 278258 cells and a mean aspect ratio of 2.1875 was prepared. The following algorithms and solvers were used for the simulation:

- Coupled Scheme
- Body Force Weighted
- Pseudo Transient Time

2.3 Fabrication of Aerographite-epoxy 3D composites

For the preparation of Aerographite composites a vacuum-assisted infiltration process as described in Ref. [35] was used. Aerographite samples were evacuated at 2 mbar and 50 °C for 45 min to desorb water. The epoxy was heated to 50 °C to decrease its viscosity and to enable better degassing and infiltration and was also evacuated. A glass desiccator with a sidewise socket was used as a vacuum container in which a mold containing the neat Aerographite could be placed. Epoxy was added using a syringe and subsequently absorbed by the Aerographite. Thereby, it fills both, the outer volume between the tetrapods as well as the inner volume of the tetrapodal hollow tubes. After infiltration, a standard curing cycle for 24 h at 30 °C and post-curing for 15 h at 80 °C was performed for all epoxy specimens. The samples were cut into cubes with 5 x 5 x 5 mm³ size.

2.4 Electrical measurements

DC electrical conductivity measurements were performed using a Keithley Source Meter 2602 in a four-wire configuration. For measurements on neat Aerographite the material was electrically contacted by pressing two plate-shaped electrodes, one of which was translationally movable, against its surfaces. To estimate the material's potential as a sensor material the electrical conductivity varies while compressing and densifying the Aerographite samples between these electrodes. The resistance parallel to the compression direction is measured in situ. It is recorded as a function of displacement in compression. The compressive force is quantified with a micro scale that measures the sample weight during compression. The data are converted afterwards into compressive stresses by taking into account the sample dimensions.

2.5 Mechanical testing of Aerographite composites

Compression tests were run on a universal test machine (Zwick Roell Z 2.5, Ulm, Germany) at 1 mm/min cross head speed. Forces were registered with a 10 kN load cell; the strain was detected by videometric measurements (Messphysik Videoextensometer ME46, Fürstenfeld, Austria) with a 75 mm focal length objective. A preload of 5 N was applied for steady start conditions for Aerographite composites.

3 Results

The analyses of the flow and temperature formation in the reactor is shown in Figure 1a. It clearly shows that the heated argon rises in the reactor. Only in the range of the samples an irregularity interrupts the otherwise very symmetrical temperature profile. The results in Figure 1b show on the rear part of silicon wafer and on the two samples in the second row a maximum temperature of approx. 1030 K. It can clearly be seen that the temperature on the front side of the silicon wafer and on the walls of the first row of samples shows a temperature of approx. 985 K. This corresponds to a temperature difference of 50 K between the first and the second row. In Figure 1c it becomes clear that the three samples of the front row are by-passed from the argon flow, which has a temperature as low as 800 K. This observation goes in hand with, the in Figure 1b in the simulation observed low surface temperature of the samples at this point. The flow rates are in a range from 0.05 to 0.2 m/s and the two rear samples are primarily impinged by the hot argon gas. The temperature of the fluid is in a range of 900 K and is significantly higher than the temperature of the fluid, in the first row of the samples. In Figure 1d is an overview of the velocity vectors in the xy-plane of the reactor. Local areas of high flow rates are the injection area, as well as the outlet of the reactor. Increased speeds will occur also below the samples. However, the two particularly striking red areas are in the upper part of the quartz glass tube.

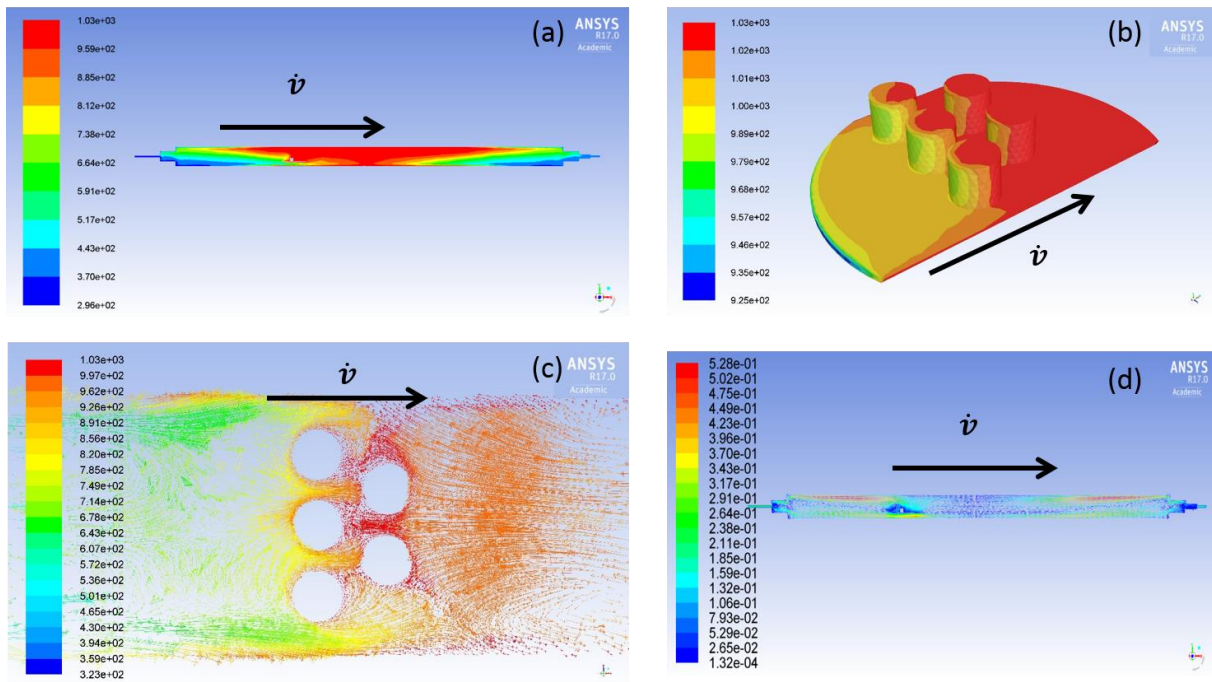


Figure 1: Temperature profile in the CVD reactor (a), of the samples (b), sample temperature vectors (c), velocity vectors over the CVD reactor (d).

In Figure 2 are shown the calculated velocity vectors for the gas flow in the reactor. The simulation results suggest that the gases flows into the reactor, initially sinks to its bottom because of the low temperature (Figure 2a). Subsequently, a large portion of the fluid flows below the silicon wafer, while a small part is deflected upwards against the specimens, as shown in Figure 2b. In the heated middle of the reactor (Figure 2c) very slow behavior of the flow velocities can be observed. Here the fluid is heated and rises up. It is remarkable that in this area almost a symmetrical distribution of the velocity vectors can be observed, so that partly the heated gas flows towards the upper quartz glass wall and partly surpasses specimens. In this range, the fluid reaches its maximum velocity of approximately 0.5 m/s. On the inner wall of the reactor, the fluid cools down and sinks towards the bottom. At the reactor outlet (Figure 2d) most of the argon gas leaves the reactor, while another part flows back into the hot area of the furnace. This behavior shows the influence of convection during the process. Normal tube flow is only present in the injection area Figure 2a and in the process of leaving the reactor Figure 2d.

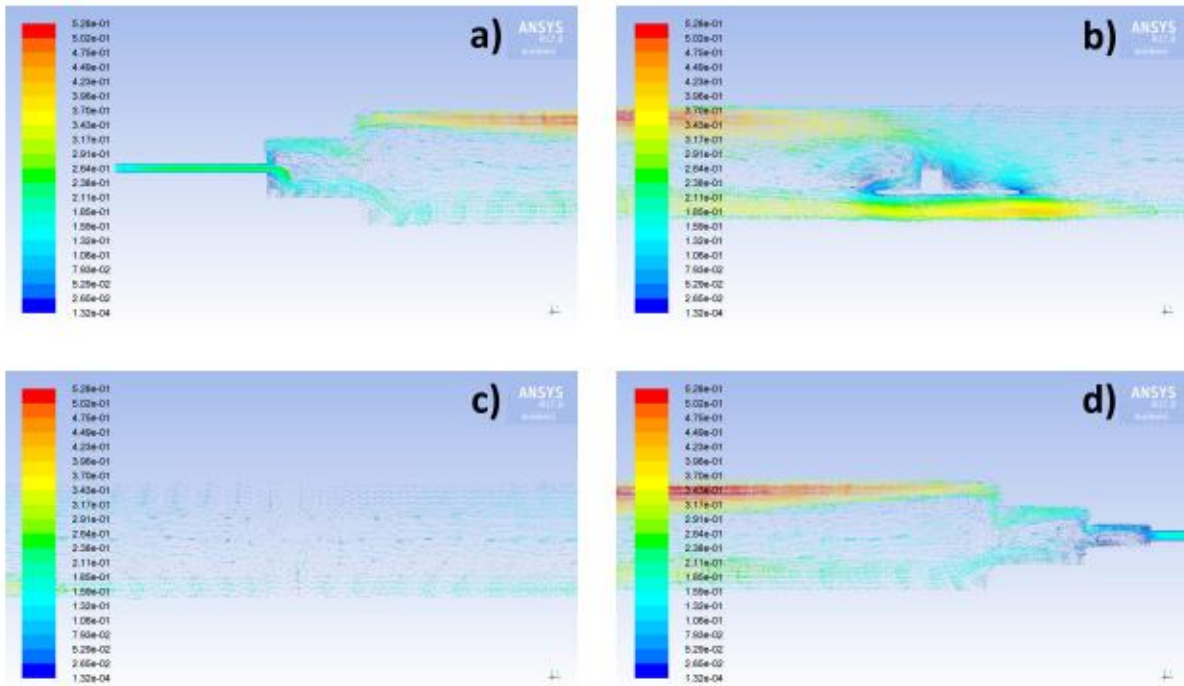


Figure 2: Velocity vectors inlet (a), sample position (b), reactor center (c), outlet (d).

Figure 3 shows in SEM images the formation of the Aerographite morphology together with a schematic model describing the transition from ZnO to the 3D graphitic structure during the interrupted synthesis. Figure 3a shows the tetrapodic structures of the neat zinc oxide templates in various magnifications. The average tetrapod arm length is 40 μm , the diameter about 2 μm . The synthesis was terminated after 15 minutes, 30 minutes, 45 minutes and 60 minutes during the 1st phase as shown in Figure 3b-e. Once the carbon source and hydrogen are injected into the reactor, a homogenous deposition of carbon can be observed on the tetrapods (Figure 2b). At first, no reaction takes place. Later a degradation of the ZnO structure with the simultaneous formation of the carbon shells can be observed. The transformation process begins on the base of the tetrapod arms (Figure 3c) and continues with time towards the tip (Figure 3d and 3e). The growth of the carbon structure into Aerographite begins at the energetically favorable points, the corner between the individual tetrapod arms, as also reported for other materials [8,9,20,21]. The tetrapodic structure itself is retained over the entire reaction time. At the end of the reaction time (135 min) a tetrapodic carbon structure remains with its characteristic thin-walled morphology (Figure 3f). In the second synthesis phase at 900 °C the remaining residues of ZnO are removed with hydrogen by the reduction into H₂O and gaseous Zn via chemical etching.

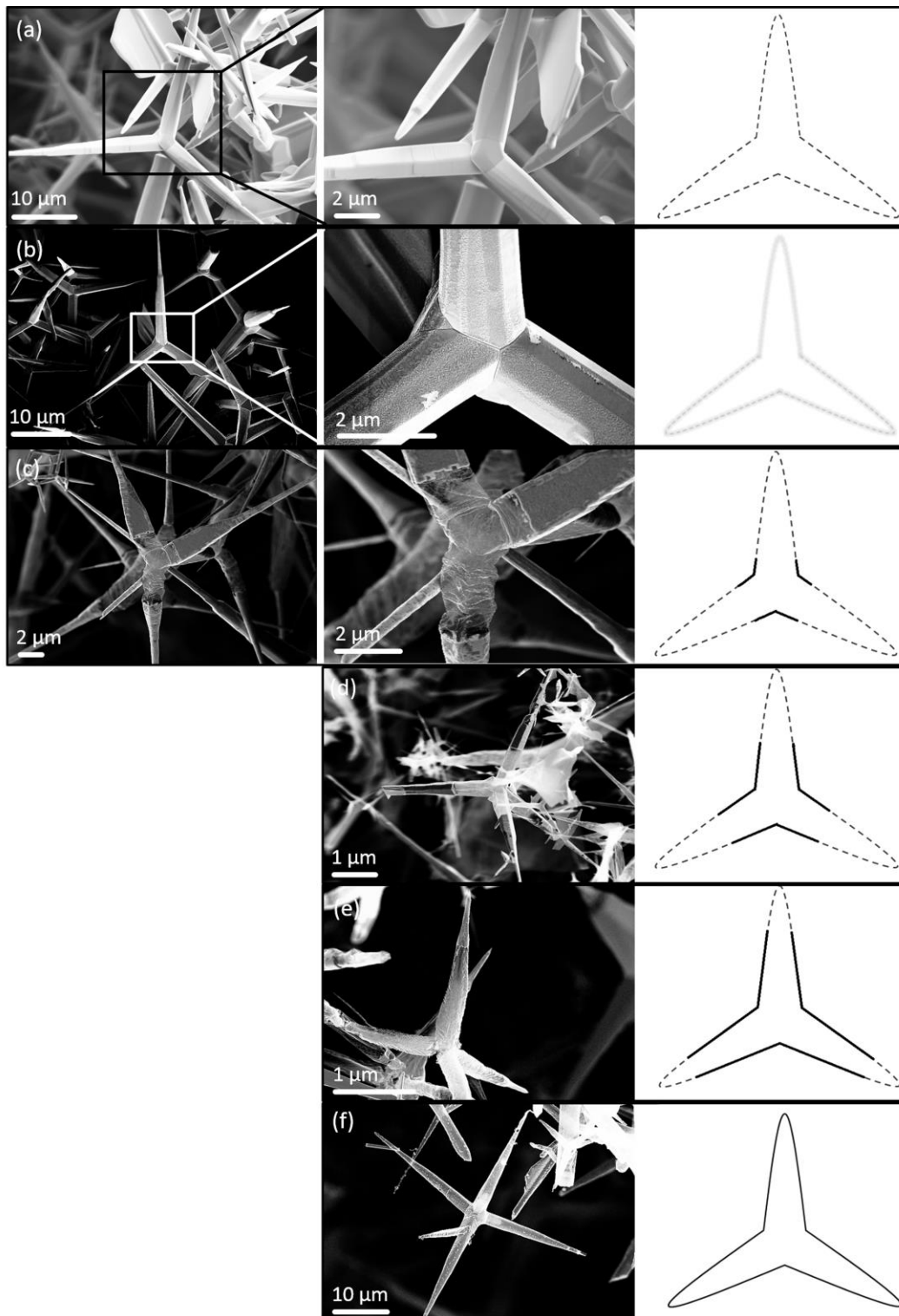


Figure 3: SEM images of zinc oxide templates (a), interrupted synthesis during the 1st phase: 15 min (b), 30 min (c), 45 min (d), 60 min (e) and after the entire synthesis 135 min (f). The figure includes a schematic demonstrating the growth mechanism.

The DC electrical conductivity of the neat Aerographite used in the composites and of the resulting composites is displayed in Figure 4a. For all samples the conductivity of the as prepared Aerographite is very similar to that of the composite's conductivity, showing that the epoxy does not cause damage to the structure as the Aerographite's network retains its electrical properties. Conductivity values are between 1.6 and 8.7 S/m. These values are

orders of magnitude higher than conductivities found in CNT composites [37-39]. Thus, we can conclude that the tunneling resistance, which dominates in carbon black or CNT composites, is negligible and the overall conductivity of the Aerographite composite is dominated by the direct three dimensional structure with interconnections between the tetrapods.

The Young's modulus of neat Aerographite was evaluated as a function of density (Figure 4b). It shows a linear correlation with the density and values between 0.08 kPa and 67.8 kPa. Ashby [40] introduced for open cell foams a power dependence of the Young's modulus on the density. This is confirmed by a number of studies on aerogels [41-44]. The linear correlation of the modulus of Aerographite can be related to the relatively low number of interconnections between the tetrapods. The stiffness of the sample might mainly be influenced by the bending stiffness of the single tetrapod arms.

In Figure 4c is plotted the compressive stress of neat Aerographite. It shows an antiproportional behavior compared to the resistance. For all samples an increase in stress is detected. For the two lightest of the four samples shown, this increase is small and almost linear. With higher density we observe a declining curve. The small increase in stress can be explained with the capability to dissipate energy while being compacted by yielding and folding of the structure for the samples with the lowest density. For the heaviest structure with 13.9 mg/cm^3 this phenomenon is less pronounced, which results in a steeper stress increase. The appearance of a declining curve for the heaviest sample of Aerographite is expected to be due to the stiffness of the tetrapods which does not allow a constant compression rather than a sudden instability and buckling of the structure. That causes the observed flattening of the curve. Generally, the stresses needed to compress the Aerographite are noticeably small, which demonstrates its ability to act as a highly force sensitive sensor material.

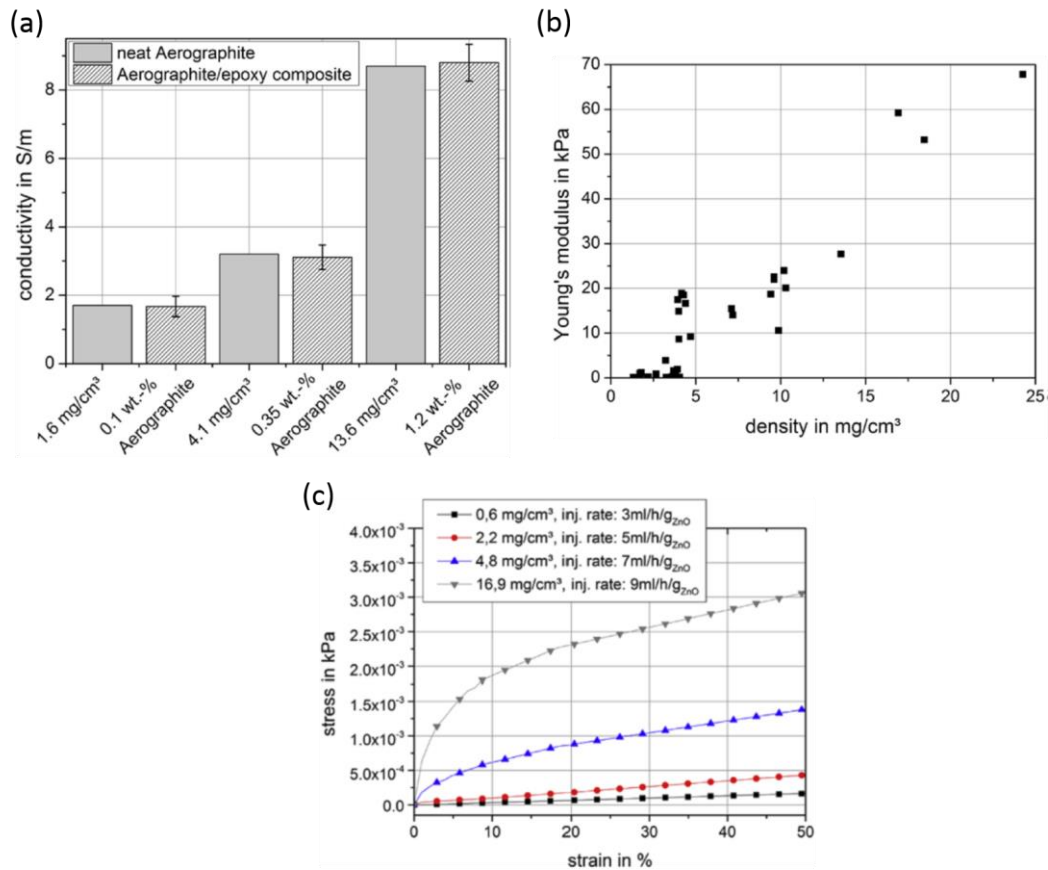


Figure 4: DC conductivity of Aerographite and corresponding epoxy composite (a), compressive Young's modulus of neat Aerographite as a function of as synthesized density (b), stress-strain curves of four neat Aerographite samples with different densities under compressive load (c).

4 Conclusion

This study shows that the growth of Aerographite is based on an epitaxial mechanism with a simultaneously catalytic graphitization of amorphous carbon into graphitic layers with zinc as catalyst. The analysis of the interrupted syntheses via SEM and TEM is a powerful tool to investigate these mechanisms. The reaction begins at the energetically favorable positions of the structure. The conversion or rather the replication into the carbon structure starts at the base of the tetrapod arms and continues to its tip. Therefore one can describe the CVD process also as a “replica CVD process” (rCVD). Furthermore, we could show. In the DC conductivity tests Aerographite shows a high initial conductivity between 0.15 and 10.2 S/m. The conductivity is proportionally depending on the sample density with a factor of 0.8. Furthermore, the samples exhibit a distinct piezoresistive behavior as their resistance decreases significantly with increasing compressive deformation. The young's modulus reaches values between 0.08 kPa and 67.8 kPa and shows a linear correlation with density. This makes the material applicable as an ultra-lightweight and vibration robust sensor material, already reacting to very small forces.

Acknowledgement

We gratefully acknowledge project funding by the German Research Foundation (DFG) under SCHU 926/25-1 and the European Union Seventh Framework Program under grant agreement n°604391 Graphene Flagship.

References

- [1] Mishra Y.K., Kaps S., Schuchardt A., Paulowicz I., Jin X., Gedamu D., et al., Fabrication of macroscopically flexible and highly porous 3D semiconductor networks from interpenetrating nanostructures by a simple flame transport approach, *Part. Part. Syst. Charact.* 30 (9) (2013) 775-783.
- [2] Mecklenburg M., Schuchardt A., Mishra Y.K., Kaps S., Adelung R., Lotnyk A., et al., Aerographite: ultra lightweight, flexible nanowall, carbon microtube material with outstanding mechanical performance, *Adv. Mater.* Deerf. Beach, Fla.) 24 (26) (2012) 3486-3490.
- [3] Yacaman M. J., Yoshida M. M., Rendon L., Santiesteban J.G., Catalytic growth of carbon microtubules with fullerene structure, *Appl. Phys. Lett.* 62 (1993) 657-659.
- [4] Endo M., Takeuchi K., Igarashi S., Kobori K., Shiraishi M., Kroto H.W., The production and structure of pyrolytic carbon nanotubes (PCNTs), *J. Phys. Chem. Solids* 54 (1993) 1841-1848.
- [5] Radushkevich L., Lukyanovich V., O strukture ugleroda, obrazujucesja pri termiceskom razlozenii okisi ugleroda na zeleznom kontakte, *Zhurnal Fiz. Khimii.* 26 (1952) 88-95.
- [6] Iijima S., Helical microtubes of graphitic carbon, *Nature* 354 (1991) 56-58.
- [7] Iijima S., Growth Model of Carbon Nanotubes, *Physical Review Letters* 69 (1993) 3100-3103.
- [8] Iijima S., Growth of carbon nanotubes, *Materials Science and Engineering B19* (1993) 172-180.
- [9] Zhang J., An Hua P., Wang X., Wang Z., Structural evolution and growth mechanism of graphene domains on copper foil by ambient pressure chemical vapor deposition, *Chemical Physics Letters* 536 (2012) 123-128.
- [10] Wang S., Qiao L., Zhao C., Zhang X., Chen J., Tian H., et al., A growth mechanism for graphene deposited on polycrystalline Co film by plasma enhanced chemical vapor deposition, *New Journal of Chemistry* 37 (2013) 1616-1622.
- [11] Hashimoto H., Naiki T., High temperature gas reaction specimen chamber for an electron microscope, *Jpn. J. Appl. Phys.* 7 (1968) 946-.
- [12] Baker R.T.K., Harris P.S., Controlled atmosphere electron-microscopy. *J. Phys. E* 5, (1972) 793-797.
- [13] Boyes E. D., Gai P. L., Environmental high resolution electron microscopy and applications to chemical science, *Ultramicroscopy* 67 (1997) 219-232.
- [14] Sharma R., Iqbal Z., In situ observations of carbon nanotube formation using environmental transmission electron microscopy, *Applied Physics Letters* 84 (6) (2004) 990-992.
- [15] Sharma R., Rez P., Treacy M.M.J., Stuart S.J., In situ observation of the growth mechanisms of carbon nanotubes under diverse reaction conditions, *Journal of Electron Microscopy* 54 (3) (2005) 231-237.
- [16] Feng X., Chee S.W., Sharma R., Liu K., Xie X., Li Q., et al., In Situ TEM Observation of the Gasification and Growth of Carbon Nanotubes Using Iron Catalysts, *Nano Res.* 4 (2011) 767-779.
- [17] Yoshida H., Takeda S., Elucidation of the origin of grown-in defects in carbon nanotubes, *Carbon* 70 (2014) 266-272.
- [18] Phokharatkul D., A. Wisitsoraat D., Lomas T., Tuantranont A., 3D hollow carbon nanotetrapods synthesized by three-step vapor phase transport, *Carbon* 80 (2014) 325-338.

- [19] Chen Z., Ren W.C., Gao L., et al., Three-dimensional flexible and conductive interconnected graphene networks grown by chemical vapour deposition, *Nat Mater* 10 (2011) 424–428.
- [20] Gui X., Wei J., Wang K., Cao A., Zhu H., Jia Y., et al., Carbon Nanotube Sponges, *Adv. Mater.* 22 (2010) 617–621.
- [21] Choy K.L., In: Nalwa H.S., editor, *Handbook of nanostructured materials and nanotechnology*, Vol.1: synthesis and processing. San Diego (CA): Academic Press; 2000. p. 533.
- [22] Lamprecht C., Taale M., Paulowicz I., Westerhaus H., Grabosch C., Schuchardt A., et al., A Tunable Scaffold of Microtubular Graphite for 3D Cell Growth, *ACS applied materials & interfaces* 8 (2016) 14980-14985.
- [23] Chandrasekaran S., Liebig W., Mecklenburg M., Fiedler B., Smazna D., Adelung R., Schulte K., Fracture, failure and compression behaviour of a 3D interconnected carbon aerogel (Aerographite) epoxy composite, *Composites Science and Technology* 122 (2016) 50-58.
- [24] Garlof S., Mecklenburg M., Smazna D., Mishra Y.K., Adelung R., Schulte K., Fiedler B., 3D carbon networks and their polymer composites: Fabrication and electromechanical investigations of neat Aerographite and Aerographite-based PNCs under compressive load, *Carbon*. 111 (2017) 103-112.
- [25] Lupan O., Postica V., Mecklenburg M., Schulte K., Mishra Y.K., Fiedler B., Adelung R., Low powered, tunable and ultra-light aerographite sensor for climate relevant gas monitoring, *J. Mater. Chem. A*. 4 (2016), 16723-16730.
- [26] A. Yasmin, J.J. Luo, J.L. Abot, I.M. Daniel, Mechanical and thermal behavior of clay/epoxy nanocomposites, *Compos. Sci. Technol.* 66 (14) (2006) 2415-2422.
- [27] F.H. Gojny, M.H. Wichmann, B. Fiedler, K. Schulte, Influence of different carbon nanotubes on the mechanical properties of epoxy matrix composites - a comparative study, *Compos. Sci. Technol.* 65 (15e16) (2005) 2300-2313.
- [28] A. Moisala, Q. Li, I.A. Kinloch, A.H. Windle, Thermal and electrical conductivity of single- and multi-walled carbon nanotube-epoxy composites, *Compos. Sci. Technol.* 66 (10) (2006) 1285-1288.
- [29] S. Chandrasekaran, N. Sato, F. Trolle, R. Mülhaupt, B. Fiedler, K. Schulte, Fracture toughness and failure mechanism of graphene based epoxy composites, *Compos. Sci. Technol.* 97 (2014) 90-99.
- [30] B. Fiedler, F.H. Gojny, M.H. Wichmann, M.C. Nolte, K. Schulte, Fundamental aspects of nano-reinforced composites, *Compos. Sci. Technol.* 66 (16) (2006) 3115-3125.
- [31] T.-H. Hsieh, Y.-S. Huang, M.-Y. Shen, Mechanical properties and toughness of carbon aerogel/epoxy polymer composites, *J. Mater Sci.* 50 (2015) 3258-3266.
- [32] G. Tang, Z. Jiang, X. Li, H. Zhang, A. Dasari, Z. Yu, Three dimensional graphene aerogels and their electrically conductive composites, *Carbon* 77 (2014) 592-599.
- [33] Z. Wang, X. Shen, M. Akbari Garakani, X. Lin, Y. Wu, X. Liu, et al., Graphene aerogel/epoxy composites with exceptional anisotropic structure and properties, *ACS Appl. Mater. Interfaces* 7 (9) (2015) 5538-5549.
- [34] Y. Ni, L. Chen, K. Teng, J. Shi, X. Qian, Z. Xu, et al., Superior mechanical properties of epoxy composites reinforced by 3D interconnected graphene skeleton, *ACS Appl. Mater. Interfaces* 7 (21) (2015) 11583-11591.
- [35] X. Liu, H. Li, Q. Zeng, Y. Zhang, H. Kang, H. Duan, et al., Electro-active shape memory composites enhanced by flexible carbon nanotube/graphene aerogels, *J. Mater. Chem. A* 3 (21) (2015) 11641-11649.
- [36] Q. Zhang, X. Xu, H. Li, G. Xiong, H. Hu, T.S. Fisher, Mechanically robust honeycomb graphene aerogel multifunctional polymer composites, *Carbon* 93 (2015) 659-670.

- [37] M.H.G. Wichmann, S.T. Buschhorn, J. Gehrman, K. Schulte, Piezoresistive response of epoxy composites with carbon nanoparticles under tensile load, *Phys. Rev. B* 80 (24) (2009).
- [38] N. Hu, Y. Karube, M. Arai, T. Watanabe, C. Yan, Y. Li, et al., Investigation on sensitivity of a polymer/carbon nanotube composite strain sensor, *Carbon* 48 (3) (2010) 680-687.
- [39] R. Zhang, H. Deng, R. Valenca, J. Jin, Q. Fu, E. Bilotti, et al., Strain sensing behaviour of elastomeric composite films containing carbon nanotubes under cyclic loading, *Compos. Sci. Technol.* 74 (2013) 1-5.
- [40] M.F. Ashby, The properties of foams and lattices, *Philos. Trans. Ser. A, Math. Phys. Eng. Sci.* 2006 (364) (1838) 15-30.
- [41] T. Woignier, J. Reynes, A. Hafidi Alaoui, I. Beurroies, J. Phalippou, Different kinds of structure in aerogels: relationships with the mechanical properties, *J. Non-Crystalline Solids* 241 (1) (1998) 45-52.
- [42] R.W. Pekala, C.T. Alviso, J.D. LeMay, Organic aerogels: microstructural dependence of mechanical properties in compression, *J. Non-Crystalline Solids* 125 (1-2) (1990) 67-75.
- [43] H. Sehaqui, Q. Zhou, L.A. Berglund, High-porosity aerogels of high specific surface area prepared from nanofibrillated cellulose (NFC), *Compos. Sci. Technol.* 71 (13) (2011) 1593-1599.
- [44] R. Saliger, V. Bock, R. Petricevic, T. Tillotson, S. Geis, J. Fricke, Carbon aerogels from dilute catalysis of resorcinol with formaldehyde, *J. Non-Crystalline Solids* 221 (2-3) (1997) 144-150.